Regular Article

blood

IMMUNOBIOLOGY

CX3CR1-dependent endothelial margination modulates Ly6C^{high} monocyte systemic deployment upon inflammation in mice

Pauline Hamon, Pierre-Louis Loyher, Camille Baudesson de Chanville, Fabrice Licata, Christophe Combadière, and Alexandre Boissonnas

Sorbonne Universités, UPMC Université Paris 06, INSERM UMR 1135, CNRS ERL8255, Centre d'Immunologie et des Maladies Infectieuses, Paris, France

Key Points

- Blood monocytes are distributed between a marginated and a circulating pool.
- CX3CR1 regulates inflammatory monocyte residence into the blood vasculature during inflammation.

Two subsets of blood monocytes are commonly described in mice and humans: the classical inflammatory monocytes, which are rapidly mobilized upon inflammation in a CC-chemokine receptor 2–dependent manner, and the nonclassical blood resident monocyte subset that patrols the intraluminal side of the endothelium. Old reports suggest that blood monocytes are distributed into circulating and marginating pools, but no direct evidence of the latter has been obtained so far. Using a combination of in vivo real-time imaging and blood/tissue partitioning by intravascular staining of leukocytes, we showed that both inflammatory and resident monocytes are retained in the bone marrow vasculature, representing an important reservoir of marginated monocytes. Upon lipopolysaccharide or cecal ligation and puncture–induced peritonitis, these marginated cells are rapidly released and recruited to the peritoneum membrane lumen vasculature where they reside through CX3C-chemokine receptor 1 (CX3CR1)–dependent adherence. At a later time point, inflammatory monocytes infiltrate the spleen parenchyma but remain mainly intravascular in the vicinity of the lungs and the peritoneum. Our results show that this monocyte deployment is controlled by a CX3CR1-dependent balance between marginating and circulating monocytes and highlight that tissue infiltration is not a mandatory fate for inflammatory monocytes. (*Blood*. 2017;129(10):1296-1307)

Introduction

Monocytes (Mo) are circulating cells implicated in the steady-state immune surveillance and in the initiation of inflammation.[1] They derive from bone marrow (BM) precursors and constitutively egress toward the bloodstream, where they differentiate into 2 functional classes, in both mice and humans. In the mouse, circulating classical or inflammatory monocytes are short lived,[2] express high levels of Ly6C and the chemokine receptor, CCR2, but also express intermediate levels of the CX3C-chemokine receptor 1 (CX3CR1). Inflammatory monocytes are precursors of longer-lived patrolling monocytes that lack Ly6C and CCR2 but express higher CX3CR1.[3] BM parenchyma and spleen are known to be the main reservoirs of monocytes,[4,5] rapidly available upon inflammation. Monocyte mobilization from the BM is CCR2 dependent in the steady state as well as under inflammatory conditions.[6,7] Beyond the role of CX3CR1 in Ly6C^{low}-Mo survival,[8] the membrane-anchored form of the CX3CL1 provides a potent adhesion molecule[9,10] that contributes to slowing down monocyte egress from the marrow during myeloablative recovery.[11]

It has been suggested that monocytes are distributed between a circulating pool and a marginating pool,[12] the latter representing up to 60% of the peripheral reservoir and defined by cells in direct interaction with the endothelium. The nature and function of marginated monocytes are not defined due to their poor accessibility. Furthermore, very little is known about the mechanism that governs this equilibrium. Intravital imaging approaches have brought experimental evidence of the presence of patrolling Ly6C^{low}-Mo[1] that crawls along the luminal side of the vessels in a CD11a-dependent manner and participates in steady-state immune surveillance. Upon inflammatory stimuli, Ly6C^{high}-Mo and Ly6C^{low}-Mo are recruited in large numbers to carry out specific effector functions.[13] Lung microvasculature represents a major site for monocyte margination after lipopolysaccharide (LPS) stimulation and during sepsis.[14-16] The spleen represents another major source of monocytes. Direct visualization of the splenic monocyte reservoir was assessed, and the subcapsular red pulp identified was as their main site of residence.[4]

Herein, we used intravital imaging approach and in vivo intravascular leukocyte staining to identify and characterize the behavior of the marginating pool of monocytes in different vascular niches, in steady state and in the course of peritonitis. Our results indicate a key role of CX3CR1 in the equilibrium between vascular retention and extravasation of blood monocytes and thus in the regulation of monocyte deployment toward the periphery.

Submitted 4 August 2016; accepted 16 December 2016. Prepublished online as *Blood* First Edition paper, 23 December 2016; DOI 10.1182/blood-2016-08-732164.

The online version of this article contains a data supplement.

There is an Inside *Blood* Commentary on this article in this issue.

The publication costs of this article were defrayed in part by page charge payment. Therefore, and solely to indicate this fact, this article is hereby marked "advertisement" in accordance with 18 USC section 1734.

Methods

Mice

C57Bl6 mice were purchased from Elevage Janvier (Le Genest, Saint Isle, France). *Cx3cr1*-EGFP-Kin (*Cx3cr1*$^{gfp/+}$),[17] *Csf1r*-Gal4VP16/UAS-ECFP (MacBlue),[18] and *Ccr2*$^{-/-}$ mice were intercrossed to generate MacBlue×*Cx3cr1*$^{gfp/+}$, MacBlue×*Cx3cr1*$^{gfp/gfp}$, or MacBlue×*Cx3cr1*$^{gfp/+}$×*Ccr2*$^{-/-}$ mouse strains and bred at Pitié-Salpêtrière animal facility.

Peritonitis models

For low-dose LPS-mediated peritonitis, mice were administered intraperitoneally with or without 100 ng/kg LPS in phosphate-buffered saline (PBS). For cecal ligation and puncture (CLP) -induced peritonitis, mice were operated as previously performed.[19] In some experiments, 50 μg of CX3CR1 antagonist (F1) antagonist[20] was injected IV into sterile PBS concomitantly with LPS injection or immediately and 3.5 hours after CLP.

Blood/tissue partitioning

Intravascular CD45 labeling was performed as previously described.[21-23] Mice were injected IV with 1 μg of anti-CD45 (clone 30-F11). Two minutes after injection, blood was drawn and mice were sacrificed. Lungs and spleen were harvested and bathed in a large volume of PBS. CD45-labeled cells in all tissues were considered to be intravascular and CD45$^-$ cells were considered to be parenchymal.

Flow cytometry

Flow cytometry acquisition was performed on the fluorescence-activated cell sorter (FACS) LSRFortessa X-20 (BD, Franklin Lakes, NJ) with DIVA Flow Cytometry software, and data were analyzed with FlowJo software (Tree Star, Inc, Ashland, OR). Blood was drawn via retro-orbital puncture with heparin and directly stained with antibodies. After staining, erythrocytes were lysed with buffer containing 0.15 M NH_4Cl, 0.01 mM $KHCO_3$, and 0.1 mM EDTA and resuspended in FACS buffer containing PBS 0.5% bovine serum albumin EDTA 2 mM. BM cells were harvested by flushing out the thighbone with PBS. Peritoneal fluids were collected by peritoneal lavage with 5 mL of ice-cold FACS buffer. Lungs and spleen were harvested and digested in RPMI 1640 medium (Gibco, Invitrogen, Cergy Pontoise, France) with 1 mg/mL collagenase IV (Sigma) for 30 minutes at 37°C and dissociated through a 40-μm pore cell strainer (Becton Dickinson, Rungis, France). One-tenth of the cell suspension was incubated with 1 μg/mL purified anti-CD16/32 (2.4G2; BD Biosciences) for 10 minutes at 4°C, and then surface staining was performed by an additional 20-minute incubation with appropriate dilution of the surface marker antibodies. Cells were then washed once in FACS buffer. For chemokine binding assays, after surface staining, cells were incubated with 100 nM *m*-Fractalkine (Alexa-647; Almac, Edinburgh, Scotland) for 45 minutes at 37°C. Cell suspensions were washed once in FACS buffer and analyzed directly by flow cytometry. CX3CL1-A647 binding specificity was controlled on CX3CR1-deficient mice.

Immunofluorescence of the peritoneal membrane

After intraperitoneal lavage, a minimum of 2 cm^2 of abdominal muscle tissue including the peritoneal membrane was cut on both sides of the linea alba and was directly laid on a microscope coverslip to image the inner side of the parietal sheet of the peritoneum. Large wide field images along the linea alba were recorded with an inverted Zeiss Axio Z1 fluorescent microscope (Carl Zeiss, Oberkochen, Germany) using Zen software. Enhanced cyan fluorescent protein (ECFP) and enhanced green fluorescent protein (EGFP) signals were acquired using an ExBP 475/40, EmBP 530/50 for EGFP and an ExBP 436/25, EmBP 480/40 for ECFP light cube filters. Cell quantification was performed by counting the number of ECFP$^+$ cells at the interface between the muscular aponevrosis and the linea alba using ImageJ software (National Institutes of Health).

Results

Intravital imaging reveals a marginated pool of Ly6C^{high} and Ly6C^{low} monocytes in BM vasculature

Intravital multiphoton microscopy provides a unique opportunity to understand spatiotemporal distribution of monocytes in their physiological environment. We tracked medullar monocytes of the skull BM using the previously described MacBlue×*Cx3cr1*$^{gfp/+}$ transgenic mouse.[23] We and others previously showed that the MacBlue transgene is mainly expressed by monocyte-derived cells, whereas it is relatively absent from tissue-resident macrophages except Langerhans cells, microglia, and alveolar macrophages.[11,23,24] A combination of high-molecular-weight Rhodamin-Dextran IV injection and second harmonic generation (SHG) signal collected from the bone matrix discriminated the vasculature from the parenchymal niches of the BM (Figure 1A). ECFP$^+$ cells were distributed in both compartments, whereas EGFP$^+$ cells were only located in the parenchymal areas. Flow cytometric analysis confirmed that >90% of BM and 53% of blood ECFP^{bright} cells were CX3CR1^{low}Ly6C^{high}-Mo (CD11b$^+$F4/80$^+$Ly6G^{neg}NK1.1^{neg}Ly6C^{high}CX3CR1^{low}), and the remaining ECFP^{bright} cells represented CX3CR1^{high}Ly6C^{low} monocytes/macrophages (supplemental Figure 1A, available on the *Blood* Web site). In the BM sinusoids, we defined circulating monocytes that can be detected in a single picture of the movies, rolling monocytes that are slowed down in the lumen of the vessels, and marginated monocytes either crawling with amoeboid-like shape or completely arrested in the lumen of the vasculature (Figure 1B; supplemental Video 1).

We next compared the behavior of the marginated monocytes in wild-type (WT), *Ccr2*$^{-/-}$, and *Cx3cr1*$^{-/-}$ mutant mice. In *Ccr2*$^{-/-}$ mice, ECFP$^+$ cells in the sinusoids were visually less frequent than in WT mice (supplemental Videos 1 and 2), and the remaining cells were mostly arrested (Figure 1C). In contrast, the proportion of arrested cells was significantly reduced in *Cx3cr1*$^{-/-}$ compared with WT mice with an increased proportion of circulating and rolling cells (Figure 1C; supplemental Videos 1 and 2). Accordingly, the distribution of the cell mean velocity among arrested, crawling, and rolling cells showed an increased proportion of cells with high velocity (>6 μm/min) in *Cx3cr1*$^{-/-}$ mice compared with WT mice (Figure 1D).

To further characterize the nature of the cells present in the vasculature of the BM, we performed blood/tissue partitioning by in vivo CD45 staining.[21] This approach allowed the discrimination between circulating monocytes, collected by blood drawing, CD45$^+$ BM-intravascular monocytes, including marginated and circulating subsets, and CD45$^-$ BM-parenchymal monocytes isolated from BM extraction (Figure 1E schema). One hundred percent of circulating cells were labeled after intravascular staining (Figure 1E left). In steady-state BM, both Ly6C^{high}-Mo and Ly6C^{low}-Mo were labeled by the anti-CD45 antibody with a lower MFI compared with circulating monocytes, showing a reduced accessibility of the antibody to the cells in accordance with cell margination to the endothelium (Figure 1E right). The numbers of these intravascular BM monocytes (CD45 in vivo$^+$ cells) in 1 thighbone of WT mice were 8159 ± 7737 for Ly6C^{high}-Mo and 6758 ± 6687 for Ly6C^{low}-Mo (Figure 1F). The ratio of in vivo CD45$^+$Ly6C^{high}/Ly6C^{low}-Mo in the BM (45 ± 18.4%) was similar to the ratio in the bloodstream (45.7% ± 19.6%), suggesting no preferential margination in the BM sinusoids of 1 subset to the other (data not shown). As expected in *Ccr2*$^{-/-}$ mice, the number of intravascular BM Ly6C^{high}-Mo but not that of Ly6C^{low}-Mo was significantly reduced compared with WT. In *Cx3cr1*$^{-/-}$ mice, only

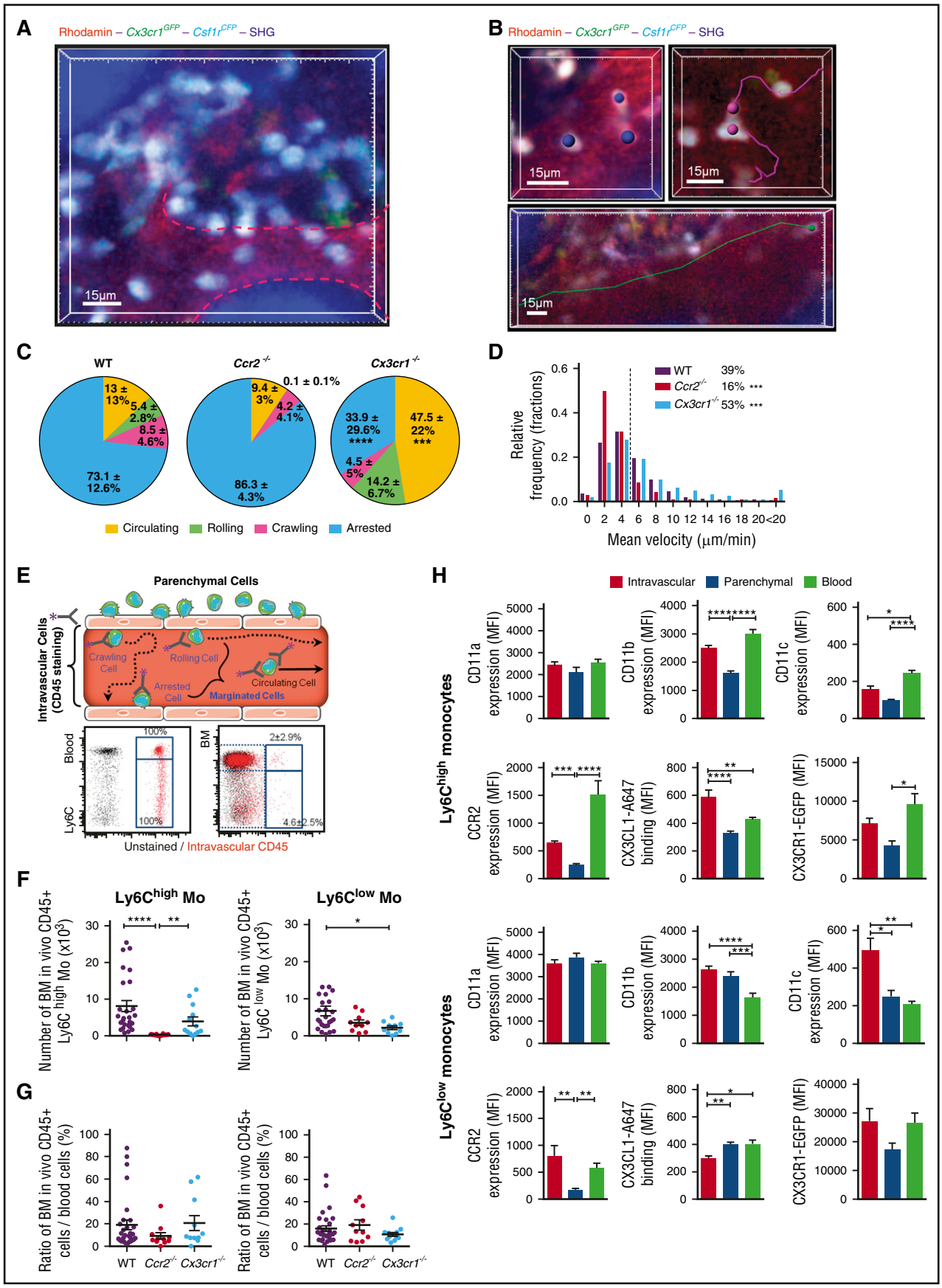

Figure 1.

the number of BM-intravascular Ly6C^{low}-Mo was significantly reduced (Figure 1F). Assuming a total blood volume of 2 mL, we estimated that BM-intravascular CD45$^+$Ly6C^{high}-Mo from only 1 thighbone represented up to 19.1% ± 23.9% (median = 9.3%) of the total circulating Ly6C^{high}-Mo and BM-intravascular CD45$^+$ Ly6C^{low}-Mo represented 15.9% ± 13.9% (median = 10.8%) of the total circulating Ly6C^{low}-Mo (Figure 1G). Considering the numerous other BM niches, this very high concentration of CD45$^+$ BM-intravascular monocytes further argues for a specific monocyte enrichment in BM sinusoids. To provide further insights on the origin of marginating monocytes, we performed intravital imaging on parabionts. One month after parabiosis between C57Bl6 (host) and MacBlue×*Cx3cr1*$^{gfp/+}$ (donor) mice, marginated ECFP$^+$ monocytes from the donor were detected in the blood vasculature of the host BM as well as within the parenchymal niches (supplemental Figure 1B-C). Flow cytometry confirmed that 66.8% ± 22% of the donor ECFP$^+$ monocytes were Ly6C^{high}, arguing that inflammatory monocytes can constitutively exchange between the vasculature and the BM parenchyma (supplemental Figure 1D). In *Ccr2*$^{-/-}$ and *Cx3cr1*$^{-/-}$ mice, the ratio of BM-intravascular to circulating Ly6C^{high}-Mo and Ly6C^{low}-Mo numbers were similar compared with WT mice, suggesting that the margination is in direct correlation with the level of circulating cell at steady state (Figure 1G).

We next investigated whether the BM-intravascular/marginated monocytes expressed differential levels of the CD11 integrins and chemokine receptors (Figure 1H) compared with peripheral blood circulating and BM-parenchymal monocytes. BM-intravascular (CD45$^+$) and circulating Ly6C^{high}-Mo expressed similar levels of the integrins CD11b and CD11a. BM-intravascular (CD45$^+$) Ly6C^{high}-Mo expressed reduced levels of CD11c and CCR2. Despite expression of the CX3CR1 reporter EGFP was lower, CX3CL1 binding was higher in BM-intravascular compared with peripheral circulating Ly6C^{high}-Mo. CD11b, CCR2, and CX3CR1 levels were increased in the intravascular (CD45$^+$) fraction of the BM compared with the parenchymal (CD45$^-$) pool. BM-intravascular Ly6C^{low}-Mo displayed increased expression of CD11b, CD11c, and CCR2 compared with its circulating counterpart but reduced level of functional CX3CR1. These different phenotypes further confirm that the BM-intravascular and peripheral circulating monocytes represent distinct pools.

We concluded that in steady-state conditions, both Ly6C^{high}-Mo and Ly6C^{low}-Mo generate a consequent marginating pool in the BM sinusoids. This reservoir is abrogated in the absence of CCR2, and its behavior depends on CX3CR1-mediated adherence to the endothelium lumen.

CCR2 and CX3CR1 control BM parenchymal and vascular monocyte release following intraperitoneal LPS injection

We next investigated the behavior of this marginating pool upon inflammation. Toll-like receptor stimulation using LPS mimics pathogen infection and permits study of the cell mobilization mechanism in a dose-dependent manner.[5] Ly6C^{high}-Mo are rapidly released from the BM until 3 hours after intraperitoneal injection of LPS (100 ng/kg) (Figure 2A). At 4 hours, the number of Ly6C^{high}-Mo recovered in the BM suggests a rehoming of mobilized cells from the blood. Neutrophils followed the same mobilization profile as Ly6C^{high}-Mo in the BM, but the number of Ly6C^{low}-Mo in the BM was barely affected by LPS challenge (Figure 2A). Surprisingly, within the first hour, the number of both circulating Ly6C^{high}-Mo and Ly6C^{low}-Mo dropped by 88% ($6.5 \pm 6.1 \times 10^4$ to $0.74 \pm 1.2 \times 10^4$) and 81% ($6.1 \pm 13.6 \times 10^4$ to $1.1 \pm 1.2 \times 10^4$), respectively (Figure 2B). The monocytopenia at 1 hour was specific as neutrophils showed an almost mirrored mobilization kinetic in the blood. Reduced margination in BM sinusoids was also observed at 1 hour for Ly6C^{high}-Mo (57% reduction of in vivo CD45$^+$ cells, from $8.2 \pm 7.7 \times 10^3$ to $3.5 \pm 3.4 \times 10^3$, $P = .04$) and to a smaller extent for Ly6C^{low}-Mo (Figure 2C). In contrast, BM-intravascular neutrophils tended to increase at 1 hour in accordance with their massive accumulation in the bloodstream (Figure 2C). The number of blood circulating Ly6C^{high}-Mo was recovered 3 hours post challenge and accumulated by fourfold ($14.9 \pm 14.2 \times 10^4$) after 4 hours according to BM release. Circulating Ly6C^{low}-Mo recovered only 4 hours after challenge, reaching approximately their number at steady state ($8.3 \pm 20.2 \times 10^4$) (Figure 2B). Circulating neutrophil numbers doubled in 1 hour and returned to basal levels at 3 hours after LPS injection. By 4 hours, the margination of both BM-intravascular Ly6C^{high}-Mo and Ly6C^{low}-Mo recovered (Figure 2C) but did not increase with the monocytosis and thus represented only 4.4% ± 3.6% (median = 3.3%) and 11.3% ± 8.3% (median = 8.6%), respectively, of the circulating monocytes of the peripheral blood (data not shown), arguing for a preferential release of Ly6C^{high}-Mo into the bloodstream. The sequential monocytopenia and monocytosis phases were observed in WT and *Cx3cr1*$^{-/-}$ mice with a slight accumulation of circulating Ly6C^{high}-Mo in CX3CR1-deficient mice compared with WT mice (supplemental Figure 2A). As expected, the Ly6C^{high} monocytosis was abrogated in *Ccr2*$^{-/-}$ mice (supplemental Figure 2A). Circulating Ly6C^{low}-Mo recovery 4 hours after LPS stimulation was not affected in both *Cx3cr1*$^{-/-}$ and *Ccr2*$^{-/-}$ mice (supplemental Figure 2A). Intravital imaging of the skull BM confirmed that marginating ECFP$^+$ monocytes were cleared from the sinusoids in WT mice and recovered with time (Figure 2D; supplemental Video 3). In *Ccr2*$^{-/-}$ mice, no accumulation of marginating ECFP$^+$ cells was observed in the BM vasculature after LPS injection (Figure 2D-E; supplemental Video 3). In CX3CR1-deficient mice, an increased accumulation of BM-intravascular cells compared with WT mice was observed after 1 hour, and even greater numbers accumulated later on (Figure 2D-E; supplemental Video 3). The ratio of crawling to rolling cells increased rapidly after LPS treatment in WT mice (Figure 2F). The mean velocity first dropped down between 60 and 150 minutes after LPS stimulation due to rapid release of the fastest

Figure 1. Intravital imaging reveals a marginated pool of Ly6C^{high} and Ly6C^{low} monocytes in BM vasculature. (A) Representative 3-dimensional (3D) 2-photon laser scanning microscopy (3D-TPLSM) pictures showing medullar monocytes in the parenchymal and vascular BM compartments of the skull in MacBlue×*Cx3cr1*$^{gfp/+}$ mice (original magnification ×573). (B) Representative tracks of vascular monocytes displaying arrested (blue; original magnification ×620), crawling (pink; original magnification ×546), and rolling (green; original magnification ×300) behaviors. Vasculature is labeled with 2-MDa Rhodamin-Dextran (red), and bone matrix is identified by SHG (blue). (C) Pie graphs represent the relative proportion of the different monocyte behaviors in each mouse strain (percent ± standard deviation [SD] from 3 to 5 independent experiments are indicated). (D) Relative frequency distribution of vascular monocyte mean velocity (data are pooled from at least 3 independent experiments; percent indicates the proportion of cells faster than 6 μm/min for each mouse strain, and Kruskal-Wallis with Dunn's multicomparisons test is performed. Statistical significance between the 2 mutants and WT mice is indicated). (E) Scheme illustrates cell behavior and intravascular staining in the BM sinusoids. Representative dot plot showing CD45 intravascular staining (red) overlaid with noninjected control mouse (black) in the blood and the BM. (F) Quantification of the blood/tissue partitioning of monocyte subsets in the different mouse strains. (G) Graphs represent the ratio of intravascular medullar monocytes in 1 thighbone to the total number of circulating monocytes. Black bars represent mean ± standard error of the mean (SEM). (Mice are pooled from at least 3 independent experiments; median is indicated in black, and Kruskal-Wallis with Dunn's multicomparison test is performed.) (H) Bar graphs show the respective marker expression (as mean fluorescence intensity [MFI]) on intravascular BM monocytes (CD45$^+$ cells after in vivo staining), parenchymal BM monocytes (CD45$^-$ after in vivo staining), and blood monocytes (CD45$^+$ cells from the blood) in WT mice. (Bars represent mean ± SEM. n = 12-14 mice out of 2 to 3 independent experiments; Kruskal-Wallis with Dunn's multicomparisons test is performed.) *$P < .05$, **$P < .01$, ***$P < .001$, ****$P < .0001$.

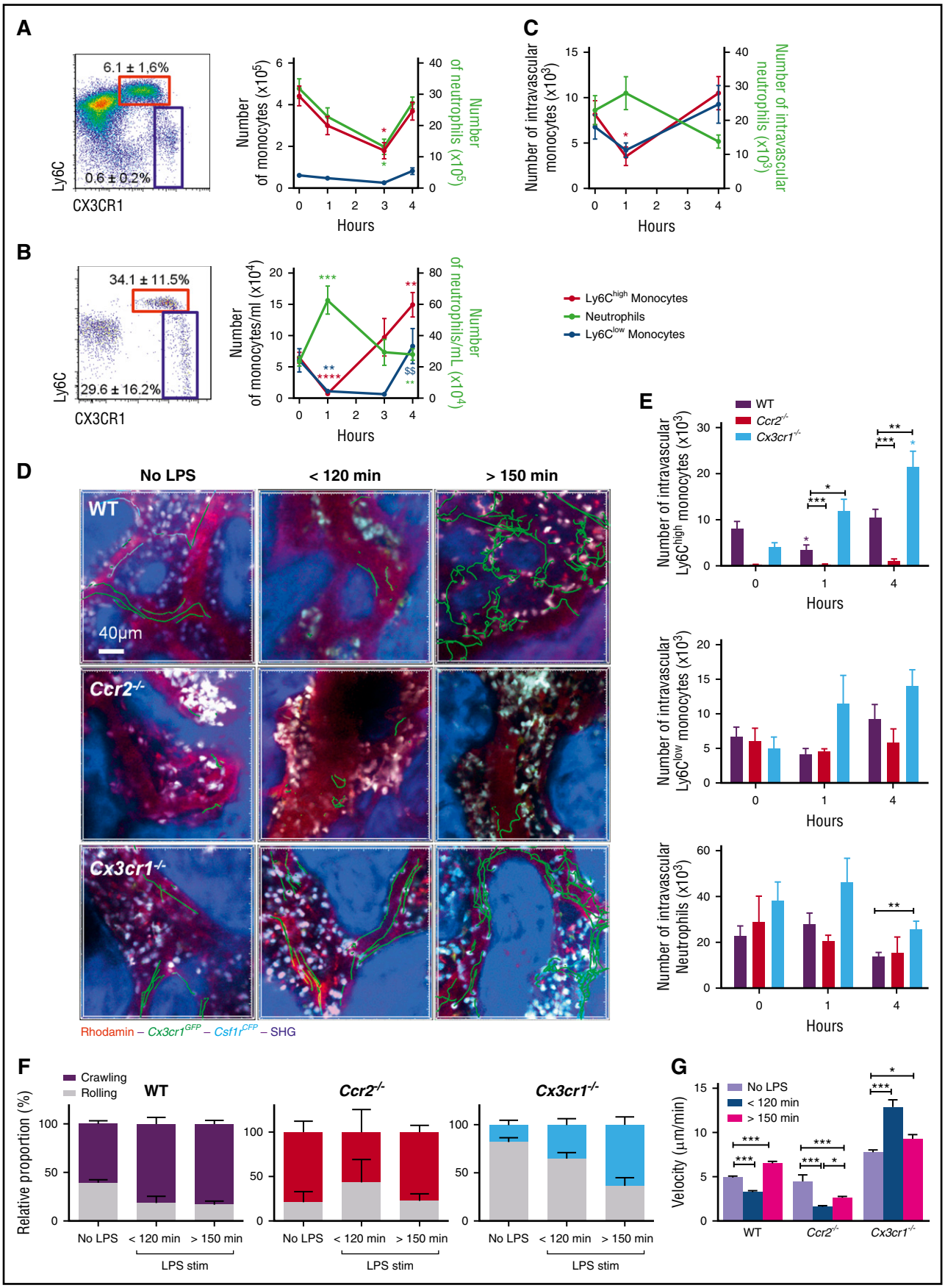

Figure 2.

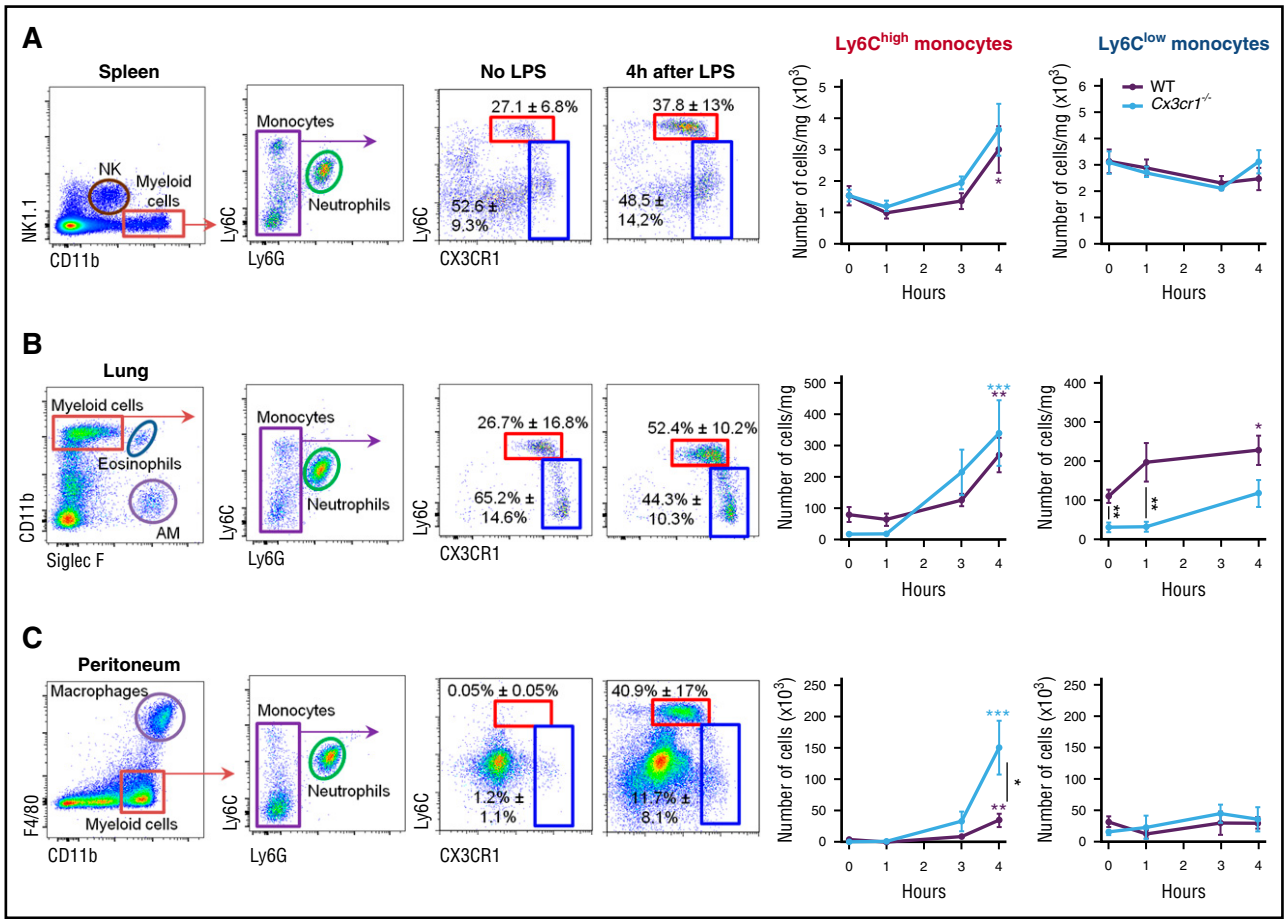

Figure 3. CX3CR1 reduces Ly6C^{high} monocyte release toward the peritoneal cavity during LPS-mediated peritonitis. Kinetics of Ly6C^{high} and Ly6C^{low} monocyte mobilization in the spleen (A), the lungs (B), and the peritoneal cavity (C) after intraperitoneal injection of 100 ng/kg LPS in MacBlue×*Cx3cr1*$^{gfp/+}$ (WT) and MacBlue×*Cx3cr1*$^{gfp/gfp}$ mice (*Cx3cr1*$^{-/-}$). Representative dot plots show the gating strategy to define Ly6C^{high} (red gate) and Ly6C^{low} monocytes (blue gate); percent ± SD are depicted. Graphs represent mean ± SEM of the absolute number per milligram of spleen or lungs and in total after peritoneal cavity lavage (n = 8-13 mice per group and per time point from at least 3 independent experiments. Kruskal-Wallis with Dunn's multicomparisons test is performed; the significance for each time point compared with untreated mice [t0] are indicated in colored *. Significance between mouse strains are indicated by black * for each time point, and Mann-Whitney test is performed). *$P < .05$; **$P < .01$; ***$P < .001$. AM, alveolar macrophages; NK, natural killer cells.

cells and increased above basal level after 150 minutes (Figure 2G). No change in the behavior of the few ECFP$^+$ monocytes present in the BM sinusoids of *Ccr2*$^{-/-}$ mice was observed, except a strong reduction in their mean velocity at early time points that persisted over time (Figure 2F-G). In *Cx3cr1*$^{-/-}$ mice, the change in the ratio between crawling and rolling cells after LPS stimulation was delayed and reduced compared with WT mice (Figure 2F). Moreover, the mean velocity of *Cx3cr1*$^{-/-}$ ECFP$^+$ cells was much higher at all time points compared with WT mice (Figure 2G). Following LPS challenge, parenchymal ECFP$^+$ cells increased their mean velocity and straightness in accordance with the parenchymal mobilization and release toward the vasculature (supplemental Figure 2B; supplemental Video 4). This acceleration was not observed in *Ccr2*$^{-/-}$ parenchymal ECFP$^+$ cells but strongly increased in the absence of CX3CR1 (supplemental Figure 2B). Our results showed that CCR2 and CX3CR1 tightly regulate medullar monocyte release by controlling both parenchymal egress and the strength of vascular margination.

Figure 2. CCR2 and CX3CR1 control BM parenchymal and vascular monocyte release following intraperitoneal LPS injection. Kinetics of Ly6C^{high} (red), Ly6C^{low} monocytes (blue), and Ly6G$^+$ neutrophils (green) mobilization in the BM (A) and the blood (B) after intraperitoneal injection of 100 ng/kg LPS in MacBlue×*Cx3cr1*$^{gfp/+}$ mice. Dot plots are gated on CD11b$^+$NK1.1$^-$Ly6G$^-$ cells (percent ± SD of the gated populations are indicated). (C) Graph shows the quantification of BM CD45$^+$ monocytes and neutrophils after intravascular staining (for all graphs, data represent mean ± SEM of absolute numbers of each subset per thighbone or per milliliter of blood quantified by flow cytometry [n = 6-12 mice for each time point out of 3 independent experiments]; Kruskal-Wallis with Dunn's multicomparisons test is performed. Only the significance for each time point compared with untreated mice [t0] is indicated). (D) Representative 3D-TPLSM images of the skull BM from MacBlue×*Cx3cr1*$^{gfp/+}$, MacBlue×*Cx3cr1*$^{gfp/+}$ *Ccr2*$^{-/-}$, and MacBlue×*Cx3cr1*$^{gfp/gfp}$ mice at different time points before and after LPS injection (original magnification ×115). Track paths of vascular ECFP$^+$ cells are represented in green. BM sinusoids are labeled by Rhodamin-Dextran (red); bone matrix is detected by SHG (blue), and monocytes are in white/cyan. (E) Flow cytometry quantification of BM CD45$^+$ monocytes and neutrophils after intravascular staining in WT, CCR2-, and CX3CR1-deficient mice bars represent mean ± SEM from 6-12 different mice per time point out of at least 3 independent experiments. Kruskal-Wallis with Dunn's multicomparisons test is performed. The significance for each time point compared with untreated mice [t0] is indicated by colored *. Significance compared to 1 h is indicated by colored $$ ($P < .01$). Significance between mouse strains is indicated by black * for each time point; Mann-Whitney test is performed. *$P < .05$; **$P < .01$; ***$P < .001$; ****$P < .0001$). (F) Quantification of the relative proportion in the number of crawling and rolling monocytes in BM sinusoids. Bars represent mean ± SEM calculated from 2 to 5 different mice per group. (G) Mean velocity of ECFP$^+$ vascular cells in the BM upon LPS injection (data are pooled from at least 3 different mice per group and per time point. One-way analysis of variance (ANOVA) with Bonferroni's multiple comparison tests is performed).

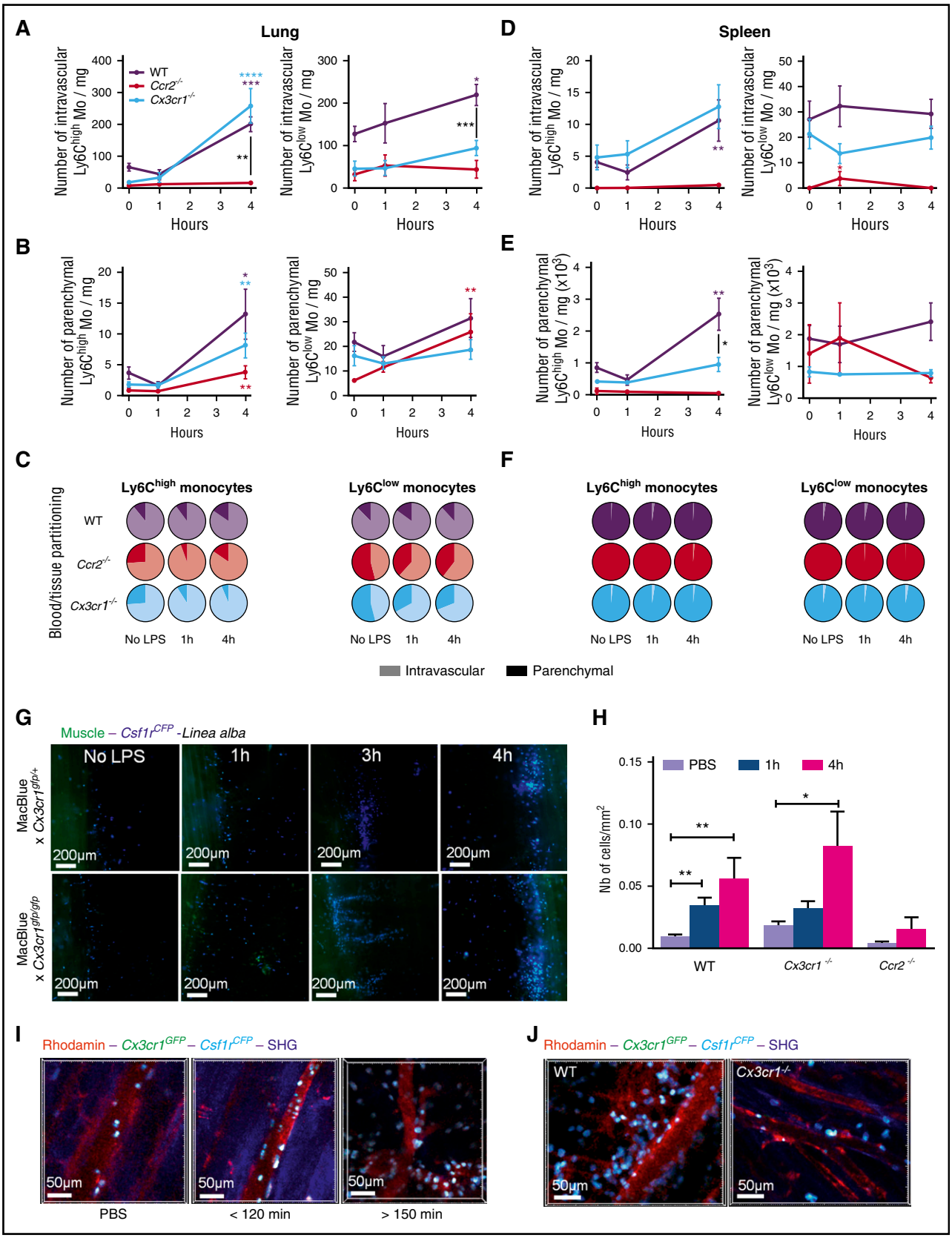

Figure 4. CCR2 and CX3CR1 control monocyte compartmentalization during inflammation. Blood/tissue partitioning of Ly6C^{high} and Ly6C^{low} monocytes in the lungs (A-C) and the spleen (D-F) are determined by in vivo CD45 intravascular staining in the different mouse strains after intraperitoneal injection of 100 ng/kg LPS in WT, CCR2-, and CX3CR1-deficient mice. (A,D) Graphs represent mean ± SEM of the absolute number per milligram of tissue of intravascular (CD45^{+}) monocytes. (B,E) Graphs represent mean ± SEM of the absolute number of parenchymal (CD45^{-}) monocytes. (C,F) Pie graphs represent the relative proportion of parenchymal (dark) and intravascular (clear) monocytes in indicated mouse strains and tissue for all graphs, n = 6-14 mice per group and per time point from at least 2 independent experiments.

CX3CR1 reduces Ly6C^{high} monocyte release toward the peritoneal cavity during LPS-mediated peritonitis

We next evaluated whether the reduced margination of CX3CR1-deficient Ly6C^{high}-Mo in the BM vasculature could have an impact on their systemic distribution.

A slight but nonsignificant reduction of Ly6C^{high}-Mo number was observed in the spleen of WT mice 1 hour after LPS injection; however, Ly6C^{high}-Mo recovered after 3 hours and further accumulated at 4 hours compared with basal value. CX3CR1 deficiency did not affect the kinetic of monocyte mobilization in the spleen (Figure 3A). The number of Ly6C^{low}-Mo in the spleen slightly diminished over time (Figure 3A). In steady-state lungs, the number of both Ly6C^{high}-Mo and Ly6C^{low}-Mo was impaired in *Cx3cr1*$^{-/-}$ mice as previously observed.[23] One hour after LPS stimulation, Ly6C^{high}-Mo numbers remained stable but strongly accumulated at 4 hours (Figure 3B). In contrast, Ly6C^{low}-Mo accumulation was weaker. Accumulation of both Ly6C^{high}-Mo and Ly6C^{low}-Mo subsets was observed in the absence of CX3CR1; however, Ly6C^{low}-Mo did not reach the level of WT mice, suggesting an important role of CX3CR1 in the homing or survival of Ly6C^{low}-Mo in the lungs (Figure 3B).

Surprisingly, in the absence of CX3CR1, Ly6C^{high}-Mo accumulated by fourfold in the peritoneal cavity 4 hours after LPS treatment compared with WT monocytes. In contrast, Ly6C^{low}-Mo numbers displayed nonsignificant variation after LPS stimulation in both mouse strains (Figure 3C).

We concluded that CX3CR1 controls Ly6C^{high}-Mo accumulation into the peritoneal cavity upon LPS stimulation.

CCR2 and CX3CR1 control monocyte blood/tissue partitioning during inflammation

We speculated that strong accumulation of Ly6C^{high}-Mo in the peritoneal cavity of CX3CR1-deficient mice could be due to a defect in their margination to the endothelium of tissue vasculatures. We previously showed that the majority of lung monocytes were trapped in the microcapillaries and in direct contact with blood and airways.[23] Blood/tissue partitioning confirmed that >90% of the lung tissue monocytes are trapped in the lung capillaries and are still labeled by in vivo CD45 staining even 4 hours after LPS stimulation (Figure 4A-C). CX3CR1 deficiency did not affect the trapping of Ly6C^{high}-Mo after LPS stimulation but affected the Ly6C^{low}-Mo, resulting in a higher proportion of parenchymal cells (Figure 4A,C). Few Ly6C^{high}-Mo and Ly6C^{low}-Mo infiltrated the lungs even at 4 hours after LPS treatment (Figure 4B-C). As a control, lung-intravascular Ly6C^{high}-Mo and Ly6C^{low}-Mo did not accumulate in *Ccr2*$^{-/-}$ mice, but the low Ly6C^{low}-Mo infiltration was still similar to WT mice (Figure 4A-C). In contrast to the lungs, the proportion of intravascular (in vivo CD45^{+}) monocytes in the splenic reservoir was minor (Figure 4C,F). Spleen-intravascular Ly6C^{high}-Mo were similar in WT and *Cx3cr1*$^{-/-}$ mice (Figure 4D); however, the splenic extravasation was slightly reduced at steady state but further significantly impaired at 4 hours in CX3CR1-deficent mice ($P = .01$) (Figure 4E). The Ly6C^{high}-Mo defect in *Ccr2*$^{-/-}$ mice was conserved in the 2 spleen compartments (Figure 4D-E). The number of spleen-intravascular Ly6C^{low}-Mo remained unchanged over time, and no significant infiltration into the spleen was observed in all mouse strains. Overall, the ratio between spleen-intravascular and spleen-parenchymal monocyte subsets was conserved over time (Figure 4F).

In order to exclude that monocyte accumulation in the peritoneal cavity of *Cx3cr1*$^{-/-}$ mice could be due to a defect in their adherence to the peritoneal membrane, we performed histological analysis by fluorescent microscopy on fresh tissue of the inner side parietal sheet of the peritoneum along the linea alba (white line) from MacBlue×*Cx3cr1*$^{gfp/+}$ and MacBlue×*Cx3cr1*$^{gfp/gfp}$ mice (Figure 4G). ECFP^{+} cell accumulation was detectable as early as 1 hour after LPS treatment. By 3 to 4 hours after LPS injection, numerous dense clusters of ECFP^{+} monocytes accumulated along the linea alba (Figure 4H). Monocyte accumulation was similar in WT and CX3CR1-deficient mice, and as expected, completely abrogated in *Ccr2*$^{-/-}$ mice (Figure 4H). Intravital imaging of the parietal sheet vasculature confirmed that circulating monocytes within the first hour following LPS injection marginated locally in the vascular lumen and strongly accumulated over time (Figure 4I; supplemental Video 5). In *Cx3cr1*$^{-/-}$ mice, this margination was almost completely abrogated and was associated with the massive accumulation in the peritoneal cavity (Figure 4J; supplemental Video 6). Our results show that inflammatory monocytes can reside in the vascular lumen of inflamed tissues and that extravasation is not a mandatory fate for monocytes.

CX3CR1 blockade induces systemic monocyte demargination

We previously showed that the F1[20] blocks monocyte CX3CL1-mediated monocyte adherence.[11] We used F1 to confirm that monocyte margination is CX3CR1 dependent and exclude potential mouse strain-associated effects. CX3CR1 blockade with F1 reduced monocyte adherence to BM endothelium 4 hours after LPS treatment, increased their mean velocity (Figure 5A-B; supplemental Video 7), and increased the number of BM-intravascular as well as circulating Ly6C^{high}-Mo compared with WT mice (Figure 5C). Monocyte margination in the proximal blood vessels of the peritoneum was also lost in F1-treated mice (Figure 5D; supplemental Video 7).

CX3CR1-dependent Ly6C^{high}-monocyte margination control monocyte deployment during CLP-induced peritonitis

We next investigated whether similar observation could be done after CLP, a more severe and clinically relevant model of sepsis. CLP induced an increased monocyte and neutrophil margination within 4 hours compared with sham-operated mice in the BM, the lungs, and the spleen (Figure 6A). BM margination was observed by real-time imaging on CLP-operated MacBlue×*Cx3cr1*$^{gfp/+}$ mice (Figure 6B). F1 treatment led to reduced adherence of monocytes as depicted by increased velocity and straightness (Figure 6C). Monocyte margination in the peritoneal vasculature after CLP was also severely impaired

Figure 4 (continued) Kruskal-Wallis with Dunn's multicomparisons test is performed, and the significance for each time point compared with untreated mice [t0] is indicated in colored *. Significances between mouse strains are indicated by black * for each time point. Mann-Whitney test is performed). (G) Representative fluorescent wide field pictures of the inner side of the parietal sheet of the peritoneal membrane (green autofluorescence) at different time point after LPS injection in MacBlue×*Cx3cr1*$^{gfp/+}$ and MacBlue×*Cx3cr1*$^{gfp/gfp}$ mice show ECFP^{+} monocytes (cyan) accumulation along the linea alba (dark area; original magnification ×20). (H) Quantification of monocyte accumulation along the linea alba in the different mouse strains (n = 3-8 mice in each group, Kruskal-Wallis with Dunn's multicomparisons test is performed for each strain). *$P < .05$; **$P < .01$; ***$P < .001$; ****$P < .0001$. (I) Representative time-lapse in vivo 3D images of the peritoneal membrane vasculature in MacBlue×*Cx3cr1*$^{gfp/+}$ shows monocyte accumulation, adhering to the endothelium at different time points after LPS injection (original magnification ×20). Vessels are labeled by Rhodamin-Dextran injection prior to imaging session (red). SHG shows conjunctive tissue of the peritoneal membrane. (J) Comparative 3D-TPLSM images showing monocyte accumulation in the peritoneal vasculature 4 hours after LPS injection in MacBlue×*Cx3cr1*$^{gfp/+}$ (WT) and MacBlue×*Cx3cr1*$^{gfp/gfp}$ mice (*Cx3cr1*$^{-/-}$) (original magnification ×106).

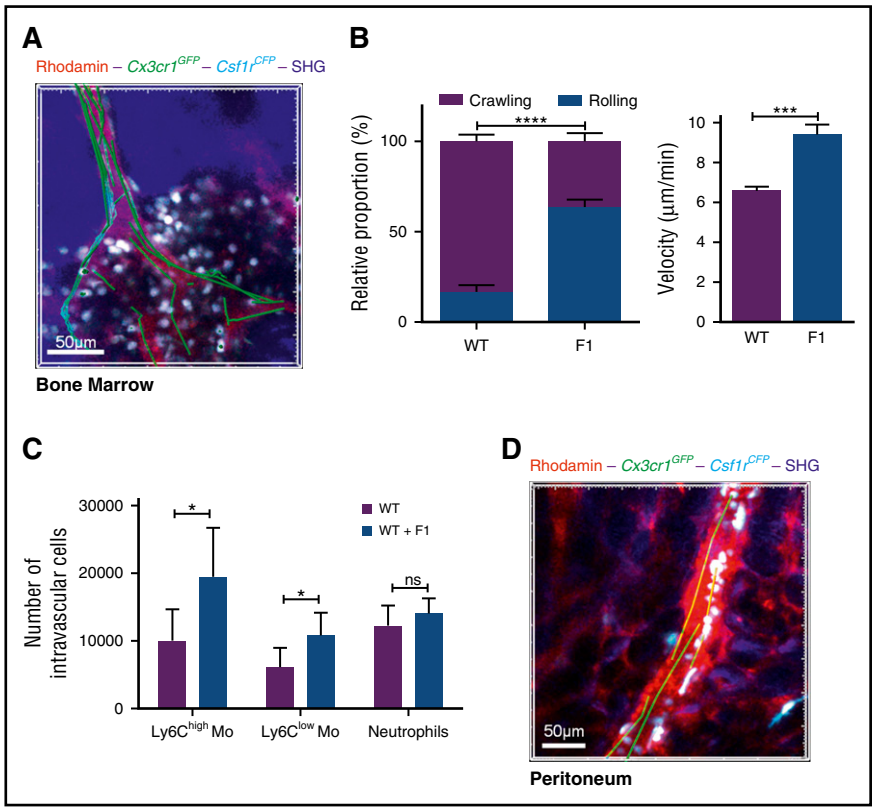

Figure 5. CX3CR1 blockade induces systemic monocyte demargination. (A) 3D-TPLSM image of the skull BM from MacBlue×*Cx3cr1*$^{gfp/+}$ 4 hours after LPS treatment in the presence of F1 (50 µg injected intraperitoneally) (original magnification ×196). Track paths (green line) showing monocyte behavior in the vasculature (red) are represented. (B) Quantification of the relative proportion of crawling and rolling monocytes and their mean velocity in the vascular lumen of the BM sinusoids from MacBlue×*Cx3cr1*$^{gfp/+}$ treated (F1) or not (WT) with CX3CR1 antagonism (bars represent mean ± SEM; data are pooled from different movies out of 2 independent experiments at least. Kruskal-Wallis with Dunn's multicomparison tests is performed). (C) Quantification by flow cytometry of intravascular Ly6C^{high}, Ly6C^{low} monocytes, and neutrophils in WT and treated (F1) after in vivo CD45 intravascular staining (bars represent mean ± SEM from at least 6 different mice per time point out of at least 2 independent experiments; Kruskal-Wallis with Dunn's multicomparisons test is performed. The significance between mouse strains is indicated by black * for each time point, and Mann-Whitney test is performed). *$P < .05$; ***$P < .001$; ****$P < .0001$; ns, nonsignificant. (D) In vivo 3D-TPLSM image of the peritoneal vasculature showing the defect in ECFP^{+} monocyte adherence to endothelium (red) 4 hours after LPS treatment in the presence of F1 (see supplemental Video 7; original magnification ×150).

by F1 treatment (Figure 6D; supplemental Video 8). Finally, this F1-mediated demargination selectively affected Ly6C^{high}-monocyte distribution between the lungs and the peritoneal cavity, with a preferential relocalization from the lungs toward the peritoneum compared with untreated CLP-operated mice (Figure 6E). We conclude that CX3CR1 is a key regulator of monocyte deployment during sepsis.

Discussion

Blood vessels have a central role in the regulation of monocyte distribution in steady state and in pathological conditions. Surprisingly, our knowledge of cell behavior in the vasculature is very limited as it is never considered a tissue of residency for leukocytes. Moreover, the characterization of blood cells is restricted to the circulating cells that are harvested from blood draw, cells adhering/marginating to the endothelial lumen being barely accessible. Three decades ago, considering the rate of BM production and the frequency of monocytes into the blood, despite a lack of experimental evidences, van Furth and Sluiter already suspected that blood monocytes might be distributed into a circulating and a marginating pool.[12] The frequency of patrolling monocytes identified by Auffray et al may represent approximately one-third of the total Ly6C^{low}-Mo pool of the vasculature,[1,25] but this may not account for the pool of marginated cells estimated by van Furth. We combined intravital imaging and blood/tissue partitioning using intravascular leukocyte labeling to demonstrate that a massive pool of vascular monocytes is marginated in the BM sinusoids at steady state. These marginated monocytes include Ly6C^{high}-Mo and Ly6C^{low}-Mo subsets in similar proportions. We extrapolated that in 1 thighbone the number of marginated cells represented ~20% of the number of circulating Ly6C^{high}-Mo. Considering all the BM niches and the lung capillaries that we have previously shown to sequester monocytes,[23] the proportion of marginated monocytes in the total vasculature of the body is increasingly being realized to be a major source of monocytes, as suggested by van Furth.[12] Interestingly, despite its role as a monocyte reservoir,[4] the spleen vasculature does not represent an important site of monocyte margination, confirming that monocytes are stocked in the parenchymal red pulp.

Patrolling activity of Ly6C^{low}-Mo in the peritoneal vasculature was previously described to be dependent of the integrin CD11a lymphocyte function-associated antigen-1 (LFA-1).[1] We compared the expression of the 3 integrins CD11a, b, and c between marginated and circulating monocytes but found no major difference in Ly6C^{high}-Mo, but did discover increased CD11b and CD11c expression between circulating and marginated Ly6C^{low}-Mo. CD11a neutralization using a specific antibody led to an almost complete depletion of both circulating and marginated monocyte subsets (data not shown). We thus could not conclude on a specific role of CD11a in monocyte margination. CX3CR1 has also been shown to be involved in the patrolling activity of Ly6C^{low}-Mo.[1,25,26] So far, the CX3CR1 expression on the 2 mouse monocyte subsets has been evaluated based on the EGFP expression in the knock-in *Cx3cr1*$^{gfp/+}$. We compared on Ly6C^{high}-Mo and Ly6C^{low}-Mo the functional expression of CX3CR1 using CX3CL1-AF647 binding with EGFP expression reflecting transcriptional activity of *Cx3cr1* promoter. Although EGFP level was lower on Ly6C^{high}-Mo compared with Ly6C^{low}-Mo, we found similar specific binding of the chemokine on both blood subsets, suggesting that the role of CX3CR1 on Ly6C^{high} could have been underestimated so far. Indeed, we observed that BM-intravascular Ly6C^{high}-Mo displayed even more CX3CL1 binding than their circulating counterparts. This result was in accordance with a role of CX3CR1 in the adherence of Ly6C^{high}-Mo in the BM vasculature. Chemokine binding confers high sensitivity due to its strong affinity for the receptor and intracellular accumulation with

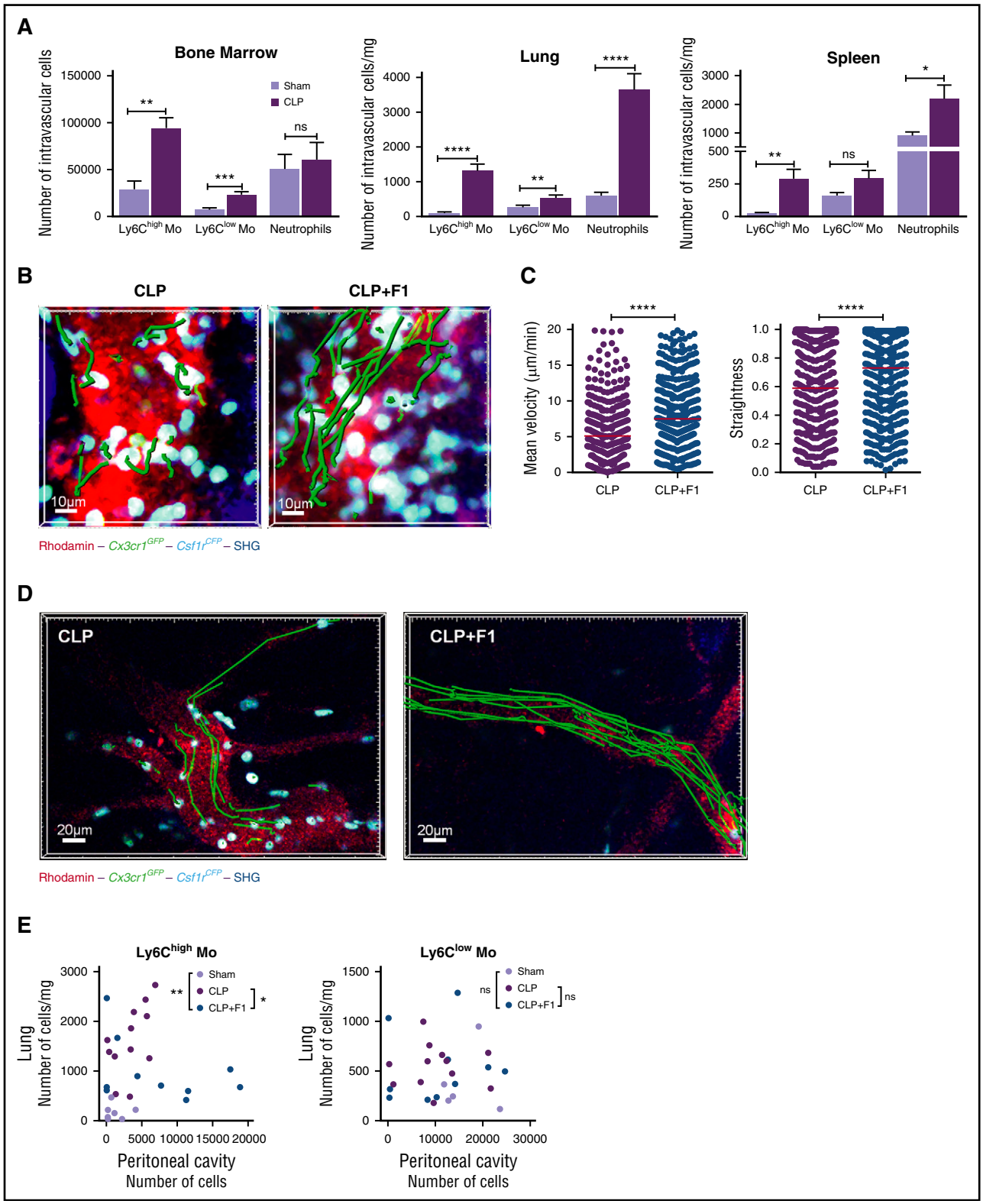

Figure 6. CX3CR1-dependent Ly6C^{high}-monocyte margination controls monocyte deployment during CLP-induced peritonitis. (A) Quantification by flow cytometry of BM, lung, and spleen-intravascular Ly6C^{high}, Ly6C^{low} monocytes, and neutrophils in Sham and CLP-operated after in vivo CD45 intravascular staining (bars represent mean ± SEM from 7 to 11 different mice per time point out of 3 to 4 independent experiments; Mann-Whitney test is performed). *$P < .05$; **$P < .01$; ***$P < .001$; **** $P < .0001$. (B) 3D-TPLSM images of the skull BM from MacBlue×*Cx3cr1*$^{gfp/+}$ 4 hours after CLP treated or not with the F1 (50 µg injected intraperitoneally) (original magnification ×440). Representative track paths are represented in green. (C) Quantification of monocyte mean velocity and straightness in the vascular lumen of the BM sinusoids from MacBlue×*Cx3cr1*$^{gfp/+}$ mice treated or not with CX3CR1 antagonism (F1) 4 hours after CLP (median is indicated in red. Data are pooled from different movies out of 3 different mice. Mann-Whitney test is performed; ****$P < .0001$). (D) In vivo 3D-TPLSM image of the peritoneal vasculature showing ECFP$^+$ monocyte adherence to endothelium 4 hours after CLP in the presence or not of F1 (original magnification ×230). Representative track paths are represented in green (see supplemental Video 8). (E) Scatter plots show the distribution of the absolute number of Ly6C^{high} and Ly6C^{low} monocytes in the lung versus the peritoneal cavity in Sham, CLP, and CLP treated with F1 4 hours after operation. Statistical differences in the distribution have been measured by a 2-way ANOVA with Bonferroni's multiple comparison tests.

receptor turnover; this observation points out that EGFP expression does not purely reflect functional CX3CR1 expression on monocyte subsets and thus requires caution for future interpretations. Similar margination was not observed in steady-state peritoneum, suggesting that Ly6C^{high} adherence to the endothelium might be different considering the anatomical locality of the vessels. Within the first hour following low-dose LPS injection in the peritoneal cavity, a drastic monocytopenia occurred. This diminution was previously observed by Shi et al in the same model of peritonitis but was not examined.[5] In contrast, the number of circulating neutrophils increased by threefold in the meantime. Interestingly, in lungs and spleen, Ly6C^{high}-Mo numbers tended to diminish at 1 hour after LPS challenge. Accumulation of Ly6C^{high}-Mo was only observed in the peritoneal membrane vasculature by in vivo imaging, suggesting a rapid relocalization of the marginated monocyte niches toward the peritoneal membrane. We thus demonstrated that BM marginated monocytes are the first released cells and (together with circulating monocytes) the most rapidly mobilized cells toward the inflammatory site. What regulates the relative proportion between circulating and marginated monocytes is unclear. High doses of LPS were shown to increase the sequestration in vascular beds,[27,28] which as a consequence reduces the proportion of circulating cells.[5]

The expected outcome of cell margination is to undergo extravasation toward the inflammatory site through sequential expression of adherent selectin and integrins.[29,30] More surprisingly, we observed that CX3CR1 expression participated in the retention of inflammatory monocytes into the endothelial lumen. This important observation led us to conclude that inflammatory monocyte infiltration into the inflamed tissue is not a mandatory fate and that blood retention might have regulatory function. In the course of cecal ligature and puncture-induced sepsis, we reported that CX3CR1-dependent Ly6C^{high}-Mo adherence to the renal endothelium exerts a protective effect against kidney injuries.[19] Herein, we extended the role of CX3CR1 in the systemic distribution of Ly6C^{high}-Mo during the early phase of acute inflammation. It is likely that monocyte adherence to the endothelium is an important feature of the compensatory anti-inflammatory response syndrome,[31,32] through interleukin-1 receptor alpha release for instance,[19] and through the cleaning of amyloid β,[33] dead cells, and potential pathogens in the vasculature.[25] Margination was still increased at day 7 in CLP-operated mice, suggesting that the regulation between marginated and circulating cells is not only a feature of acute inflammation (data not shown). In addition, we previously showed that F1 antagonist treatment can limit the development of atherosclerotic plaques by reducing monocyte adherence, which, by contrast, demonstrate a deleterious effect of CX3CR1-dependent monocyte margination in a chronic disease.[34]

Our results provide novel insights into the regulation of monocyte fate and deployment in steady-state or inflammatory conditions and, more specifically, into the role of CX3CR1 expression by the Ly6C^{high}-Mo subset. Regulating the CX3CR1/CX3CL1 axis represents an interesting approach to regulate the recruitment of inflammatory cells and modulate the outcome of the inflammatory response.

Acknowledgments

The authors thank Andrew J. Hutton for English editing of the manuscript and M. P. Rodero and C. Auffray for helpful discussions and the Plateforme Imagerie Pitié-Salpêtrière for assistance with the 2-photon microscope and the animal facility "Nouvelle Animalerie Commune." The research leading to these results has received funding from INSERM, from Centre National de la Recherche Scientifique, from Université Pierre et Marie Curie, from Fondation pour la Recherche Médicale "Equipe labelisée," from "Agence Nationale de la Recherche," project CMOS (CX3CR1 expression on monocytes during sepsis) 2015 (ANR-EMMA-050). P.H. was supported by the "Ligue Contre le Cancer."

Authorship

Contribution: P.H. designed, performed the experiments, analyzed and interpreted the data, and wrote the manuscript; P.-L.L., F.L., and C.B.d.C. performed some experiments; C.C. designed research and wrote the manuscript; A.B. supervised the study, designed and performed the experiments, analyzed and interpreted the data, and wrote the manuscript.

Conflict-of-interest disclosure: The authors declare no competing financial interests.

ORCID profiles: A.B., 0000-0002-7770-7210.

Correspondence: Alexandre Boissonnas, INSERM U1135, CNRS ERL8255, Centre d'Immunologie et des Maladies Infectieuses, 91 Boulevard de l'Hôpital, 75013 Paris, France; e-mail: alexandre.boissonnas@upmc.fr.

References

1. Auffray C, Fogg D, Garfa M, et al. Monitoring of blood vessels and tissues by a population of monocytes with patrolling behavior. *Science*. 2007;317(5838):666-670.
2. Yona S, Kim KW, Wolf Y, et al. Fate mapping reveals origins and dynamics of monocytes and tissue macrophages under homeostasis [published correction appears in Immunity. 2013; 38(5):1073-1079]. *Immunity*. 2013;38(1):79-91.
3. Sunderkötter C, Nikolic T, Dillon MJ, et al. Subpopulations of mouse blood monocytes differ in maturation stage and inflammatory response. *J Immunol*. 2004;172(7):4410-4417.
4. Swirski FK, Nahrendorf M, Etzrodt M, et al. Identification of splenic reservoir monocytes and their deployment to inflammatory sites. *Science*. 2009;325(5940):612-616.
5. Shi C, Jia T, Mendez-Ferrer S, et al. Bone marrow mesenchymal stem and progenitor cells induce monocyte emigration in response to circulating toll-like receptor ligands. *Immunity*. 2011;34(4): 590-601.
6. Tsou CL, Peters W, Si Y, et al. Critical roles for CCR2 and MCP-3 in monocyte mobilization from bone marrow and recruitment to inflammatory sites. *J Clin Invest*. 2007;117(4):902-909.
7. Serbina NV, Pamer EG. Monocyte emigration from bone marrow during bacterial infection requires signals mediated by chemokine receptor CCR2. *Nat Immunol*. 2006;7(3):311-317.
8. Landsman L, Bar-On L, Zernecke A, et al. CX3CR1 is required for monocyte homeostasis and atherogenesis by promoting cell survival. *Blood*. 2009;113(4):963-972.
9. Garton KJ, Gough PJ, Blobel CP, et al. Tumor necrosis factor-alpha-converting enzyme (ADAM17) mediates the cleavage and shedding of fractalkine (CX3CL1). *J Biol Chem*. 2001; 276(41):37993-38001.
10. Hermand P, Pincet F, Carvalho S, et al. Functional adhesiveness of the CX3CL1 chemokine requires its aggregation. Role of the transmembrane domain. *J Biol Chem*. 2008; 283(44):30225-30234.
11. Jacquelin S, Licata F, Dorgham K, et al. CX3CR1 reduces Ly6Chigh-monocyte motility within and release from the bone marrow after chemotherapy in mice. *Blood*. 2013;122(5):674-683.
12. van Furth R, Sluiter W. Distribution of blood monocytes between a marginating and a circulating pool. *J Exp Med*. 1986;163(2):474-479.
13. Shi C, Pamer EG. Monocyte recruitment during infection and inflammation. *Nat Rev Immunol*. 2011;11(11):762-774.
14. Doherty DE, Downey GP, Schwab B III, Elson E, Worthen GS. Lipolysaccharide-induced monocyte retention in the lung. Role of monocyte stiffness, actin assembly, and CD18-dependent adherence. *J Immunol*. 1994;153(1):241-255.

15. O'Dea KP, Young AJ, Yamamoto H, Robotham JL, Brennan FM, Takata M. Lung-marginated monocytes modulate pulmonary microvascular injury during early endotoxemia. *Am J Respir Crit Care Med*. 2005;172(9):1119-1127.

16. Charavaryamath C, Janardhan KS, Caldwell S, Singh B. Pulmonary intravascular monocytes/macrophages in a rat model of sepsis. *Anat Rec A Discov Mol Cell Evol Biol*. 2006;288(12):1259-1271.

17. Jung S, Aliberti J, Graemmel P, et al. Analysis of fractalkine receptor CX(3)CR1 function by targeted deletion and green fluorescent protein reporter gene insertion. *Mol Cell Biol*. 2000;20(11):4106-4114.

18. Ovchinnikov DA, van Zuylen WJ, DeBats CE, Alexander KA, Kellie S, Hume DA. Expression of Gal4-dependent transgenes in cells of the mononuclear phagocyte system labeled with enhanced cyan fluorescent protein using Csf1r-Gal4VP16/UAS-ECFP double-transgenic mice. *J Leukoc Biol*. 2008;83(2):430-433.

19. Chousterman BG, Boissonnas A, Poupel L, et al. Ly6Chigh monocytes protect against kidney damage during sepsis via a CX3CR1-dependent adhesion mechanism. *J Am Soc Nephrol*. 2016;27(3):792-803.

20. Dorgham K, Ghadiri A, Hermand P, et al. An engineered CX3CR1 antagonist endowed with anti-inflammatory activity. *J Leukoc Biol*. 2009;86(4):903-911.

21. Anderson KG, Mayer-Barber K, Sung H, et al. Intravascular staining for discrimination of vascular and tissue leukocytes. *Nat Protoc*. 2014;9(1):209-222.

22. Girgis NM, Gundra UM, Ward LN, Cabrera M, Frevert U, Loke P. Ly6C(high) monocytes become alternatively activated macrophages in schistosome granulomas with help from CD4+ cells. *PLoS Pathog*. 2014;10(6):e1004080.

23. Rodero MP, Poupel L, Loyher PL, et al. Immune surveillance of the lung by migrating tissue monocytes. *eLife*. 2015;4:e07847.

24. Sauter KA, Pridans C, Sehgal A, et al. The MacBlue binary transgene (csf1r-gal4VP16/UAS-ECFP) provides a novel marker for visualisation of subsets of monocytes, macrophages and dendritic cells and responsiveness to CSF1 administration. *PLoS One*. 2014;9(8):e105429.

25. Carlin LM, Stamatiades EG, Auffray C, et al. Nr4a1-dependent Ly6C(low) monocytes monitor endothelial cells and orchestrate their disposal. *Cell*. 2013;153(2):362-375.

26. Thomas G, Tacke R, Hedrick CC, Hanna RN. Nonclassical patrolling monocyte function in the vasculature. *Arterioscler Thromb Vasc Biol*. 2015;35(6):1306-1316.

27. Andonegui G, Bonder CS, Green F, et al. Endothelium-derived Toll-like receptor-4 is the key molecule in LPS-induced neutrophil sequestration into lungs. *J Clin Invest*. 2003;111(7):1011-1020.

28. Andonegui G, Zhou H, Bullard D, et al. Mice that exclusively express TLR4 on endothelial cells can efficiently clear a lethal systemic Gram-negative bacterial infection. *J Clin Invest*. 2009;119(7):1921-1930.

29. Soehnlein O, Lindbom L, Weber C. Mechanisms underlying neutrophil-mediated monocyte recruitment. *Blood*. 2009;114(21):4613-4623.

30. Zuchtriegel G, Uhl B, Hessenauer ME, et al. Spatiotemporal expression dynamics of selectins govern the sequential extravasation of neutrophils and monocytes in the acute inflammatory response. *Arterioscler Thromb Vasc Biol*. 2015;35(4):899-910.

31. Petit-Bertron AF, Fitting C, Cavaillon JM, Adib-Conquy M. Adherence influences monocyte responsiveness to interleukin-10. *J Leukoc Biol*. 2003;73(1):145-154.

32. Adib-Conquy M, Cavaillon JM. Compensatory anti-inflammatory response syndrome. *Thromb Haemost*. 2009;101(1):36-47.

33. Michaud JP, Bellavance MA, Préfontaine P, Rivest S. Real-time in vivo imaging reveals the ability of monocytes to clear vascular amyloid beta. *Cell Reports*. 2013;5(3):646-653.

34. Poupel L, Boissonnas A, Hermand P, et al. Pharmacological inhibition of the chemokine receptor, CX3CR1, reduces atherosclerosis in mice. *Arterioscler Thromb Vasc Biol*. 2013;33(10):2297-2305.